



Article

Describing Road Booming Noise with a Hybrid Simulation Model Using a Time Segmentation of the Excitation Load Approach

Michael Herrmann ^{1,2,*} , Jan Kralicek ², Wolfgang Stein ² and Frank Gauterin ^{1,*} ¹ Institute of Vehicle System Technology, Karlsruhe Institute of Technology, 76131 Karlsruhe, Germany² Dr. Ing. h.c. F. Porsche AG, 71287 Weissach, Germany; jan.kralicek@porsche.de (J.K.); wolfgang.stein@porsche.de (W.S.)

* Correspondence: michael.herrmann@kit.edu (M.H.); frank.gauterin@kit.edu (F.G.)

Abstract: One of the most important goals in vehicle acoustics is to describe the NVH behavior of a vehicle at sound pressure level using simulation models at an early stage of development. Different simulation models and methods are used for this purpose. To balance the advantages and disadvantages of the different methods, it is important to combine the simulation models. For the virtual description of the road booming noise behavior of a vehicle passing a rough road, we use a multibody simulation model excited with the elevation profile of the road in the time domain. To calculate the sound pressure inside the vehicle, the internal chassis forces of the multibody simulation model are combined with a finite element body model including the air cavity inside the cabin. The methodology for combining the chassis forces and body transfer functions to calculate the sound pressure is first validated using test data and then applied to the simulation data. The correlation of the calculated sound pressure based on test data ($\rho = 0.96$) and based on simulation data ($\rho = 0.90$) compared to a microphone measurement is very high.

Keywords: acoustic; vehicle; road; booming; noise; simulation; model; NVH



Citation: Herrmann, M.; Kralicek, J.; Stein, W.; Gauterin, F. Describing Road Booming Noise with a Hybrid Simulation Model Using a Time Segmentation of the Excitation Load Approach. *Vehicles* **2021**, *3*, 469–479. <https://doi.org/10.3390/vehicles3030028>

Academic Editor: Jiliang Mo

Received: 7 July 2021

Accepted: 3 August 2021

Published: 4 August 2021

Publisher's Note: MDPI stays neutral with regard to jurisdictional claims in published maps and institutional affiliations.



Copyright: © 2021 by the authors. Licensee MDPI, Basel, Switzerland. This article is an open access article distributed under the terms and conditions of the Creative Commons Attribution (CC BY) license (<https://creativecommons.org/licenses/by/4.0/>).

1. Introduction

A major goal of vehicle acoustics is to describe the vehicle's noise behavior using simulation models [1]. Increasingly complex models and simulation methods are being used for this purpose [1]. The models range from individual components or subsystems to the entire vehicle. Since different excitation mechanisms of acoustic phenomena or certain parameters can only be described with a wide variety of simulation methods, it is essential to cleverly combine these methods [1]. It is important to note that the final criterion for developing vehicle acoustics is always the subjective perception of a customer [1]. It is, therefore, crucial to be able to simulate the noise behavior of a vehicle at sound pressure level.

Due to the automotive industry's shift towards electric drive concepts, the acoustic behavior of a vehicle is becoming increasingly important [2,3]. The absence of the combustion engine noise and the loss of its masking effects causes an increased relevance of road noise [2,3]. Thereby, it can be divided into different categories, such as low frequency road booming noise or low to mid frequency rolling noise. We focus on the road booming noise, which is mainly excited by non-uniform road profiles [4,5]. The excitation introduced into the chassis primarily causes the rear axle to resonate in a pitching and lifting motion [6–8]. The vehicle's body responds with a coupled vibration mode formed by the first bending mode of the body, a rigid-body motion of the tailgate and the first longitudinal mode of the air cavity [8]. Passengers experience this phenomenon as ear pressure and booming noise at low frequencies [4,9]. One development goal is to evaluate the road booming noise behavior of a vehicle at sound pressure level using a complete vehicle simulation model. For this purpose, different approaches and simulations model are used.

Uhlar (2020) [10] investigates the booming sensitivity of a vehicle and achieves an improvement by reducing the dynamic chassis forces. For this purpose, a complete vehicle simulation model (multibody simulation, MBS) in combination with design of experiments is used to reduce the dynamic forces. However, there is no simulation at sound pressure level. Excitation on a dynamometer is used as the load case for the simulation.

Bijwe et al. (2011) [11] also optimize the booming sensitivity by geometry changes to the chassis. This is done by using a complete vehicle simulation model (finite element method, FEM) to perform a modal analysis and calculate transfer functions from the chassis connection points on the vehicle's body (unit force) to the passengers (sound pressure). However, only one point is excited individually with a unit force (equals a noise transfer function calculation) one after the other and no real or simulated chassis excitation is used. Thus, an optimization of individual transfer functions is performed and no evaluation on sound pressure level with chassis excitation is done.

Sung et al. (2011) [12] investigate drivetrain-induced booming, which is very similar to road booming noise. Drivetrain vibrations excite the vehicle's body and thus produce a similar booming noise as when excited by the chassis driving on a bad road. A finite element trimmed body simulation model with an air cavity is used for the research. The model is excited with a unit force at the connection points of the drivetrain on the vehicle's body and the sound pressures at the seat positions are calculated. This method is equivalent to the calculation of the transfer functions from the chassis connection points to the seats positions from the road booming noise investigations of Bijwe et al. (2011) [11]. Optimizations are then performed on the structure of the trimmed body to improve individual transfer paths. The identified modifications were tested and validated in a vehicle measurement.

The commonality of the three approaches explained is that a so-called equivalent load case is required, and no simulation was done to calculate the sound pressure level with real or simulated chassis excitation. Equivalent load cases are mainly used, for example, to convert and simplify real road excitations, which are often stochastic, into deterministic excitations. Since the setup and use of MBS and FE simulation models has been state of the art for a long time and is constantly applied, this paper focuses mainly on the possibilities how the different models can be combined. Our goal is to combine the advantages of MBS and FE simulation to evaluate the low-frequency road booming noise behavior of a vehicle at sound pressure level with real or simulated chassis excitation.

2. Materials and Methods

This section describes the test vehicle, the test track, the used measurement methods, different approaches to calculate the sound pressure, and the used simulation models.

2.1. Research Vehicle and Test Track

A station wagon is chosen as the test vehicle as these are more sensitive to road booming noise than sedans [13].

As a test track, we use a replica of an approximately 750 m long section of a road with a non-uniform road profile. The road unevenness is characterized by a waviness factor w of 2.0 and an unevenness level $\Phi_h(\Omega_0)$ of 33.0 and therefore corresponds to a poor subjective rating for evenness (category D) [14]. The elevation profile of the track is mapped and can be used as an excitation of our chassis simulation model (see Section 2.4.2).

2.2. Measurement Equipment and Methods

In this section, we describe the methods used to determine noise transfer functions of a vehicle's body, the calculation of chassis internal forces and different approaches to calculate the sound pressure.

2.2.1. Determining Noise Transfer Functions of a Vehicle Using Impact Measurement

To characterize the acoustic transmission behavior of a vehicle's body, it is usually examined in its trimmed body shape. We removed the engine, the powertrain, the exhaust system, the front axle, and the rear axle.

We use an impact hammer (PCB 086C03) to induce force into the body in one direction at the chassis connection points. The transmitted forces are recorded in a measuring system (Simcenter SCADAS Mobile). Microphones (Bruel & Kjaer Type 4189) on the vehicle's seat positions record sound pressures in response to the excitation signal. Subsequently, all signals are transferred into the frequency domain by applying an FFT and the sound pressures $p_j(\omega)$ are divided by the forces $F_i(\omega)$. The results are noise transfer functions $\underline{NTE}_{i,j}(\omega)$ from the force initiation point i to the seating positions j :

$$\underline{NTE}_{i,j}(\omega) = \frac{p_j(\omega)}{F_i(\omega)} \quad (1)$$

We repeat this process for each connection point between the chassis and the body in three directions.

2.2.2. Determination of Chassis Internal Forces

To determine the internal forces between the chassis and the vehicle's body, we use the bearing stiffness method [7]. In the first step, the relative displacements that occur within the chassis bearings are calculated:

$$s_{rel,i}(t) = s_{chassis,i}(t) - s_{body,i}(t) \quad (2)$$

The relative displacement $s_{rel,i}$ results from the difference just before ($s_{chassis,i}$) and just after ($s_{body,i}$) the bearing. These are obtained by double integration (high-pass filter 0.2 Hz) of the accelerations measured with accelerometers (PCB 354C03). After applying an FFT, one gets the relative displacement in the frequency domain as a complex number $\underline{s}_{rel,i}(\omega)$. The index i stands for the connection points between the body and chassis. The internal force $F_i(\omega)$ then results from multiplying the relative displacement by the complex dynamic stiffness of the bearing $\underline{c}_{dyn,i}(\omega)$:

$$F_i(\omega) = \underline{s}_{rel,i}(\omega) * \underline{c}_{dyn,i}(\omega) \quad (3)$$

We repeat this calculation for the connection points of the rear axle to the vehicle's body in three directions.

The dynamic stiffness of the bearing $\underline{c}_{dyn,i}(\omega)$ is determined on an elastomer test rig. The bearing is mounted in the test rig in the corresponding direction and excited with a hydraulic cylinder. A load cell in the setup enables the measurement and calculation of the dynamic forces in the bearing core. A path-constant sine signal is used as excitation via the hydraulic cylinder at individual frequencies. The amplitude of the signal corresponds approximately to the excitation that occurs at the bearing during the passage of a rough road section in real driving operation. The test setup for determining the dynamic bearing stiffness is described and explained in detail in [15].

2.3. Calculation of the Sound Pressure with Different Approaches

If one wants to calculate the sound pressure in the cavity of a vehicle when driving on a test track, it must be considered how the excitation forces, along the test track, can be described. Two possible methods will be presented below [16].

2.3.1. Averaging of the Excitation Spectrum in the FFT Algorithm

One possible approach is to average the excitation spectra along the entire test track [16]. The track is divided into several windows. For each window, the relative displacements are calculated, according to Equation (2), and converted into the frequency

domain. For amplitude accuracy, we use a flattop windowing ($a_0 = 0.216; a_1 = 0.417; a_2 = 0.277; a_3 = 0.084; a_4 = 0.007$) with an overlap of 90%. The relative displacements are then averaged (RMS) over all windows and multiplied by the dynamic stiffness of the bearings. The result is a set of internal forces $E_i(\omega)$ at the connection points between the chassis and the body averaged along the track. It should be noted that this also averages the phase information of the forces along the track. Then the sound pressure for each single transfer path is calculated as follows:

$$p_{i,j}(\omega) = E_i(\omega) * NTF_{i,j}(\omega) \tag{4}$$

The sound pressure $p_{i,j}(\omega)$ is the result of multiplying the internal force $E_i(\omega)$ by the corresponding transfer function $NTF_{i,j}(\omega)$ of the vehicle's body. The index i describes the excitation position, e.g., rear shock absorber left, the index j the sound pressure at a seat position, e.g., driver's seat. Finally, all individual paths are added up in phase to a total sound pressure $p_{total,j}(\omega)$:

$$p_{total,j}(\omega) = \left| \sum_1^i p_{i,j}(\omega) \right| \tag{5}$$

It is important, that the magnitude of the complex sound pressures is only formed as the last step in the total sound pressure.

2.3.2. Time Segmentation of the Excitation Load

Another way to calculate the sound pressure is the time segmentation of the excitation load approach [16]. Figure 1 shows the method for calculating the sound pressure.

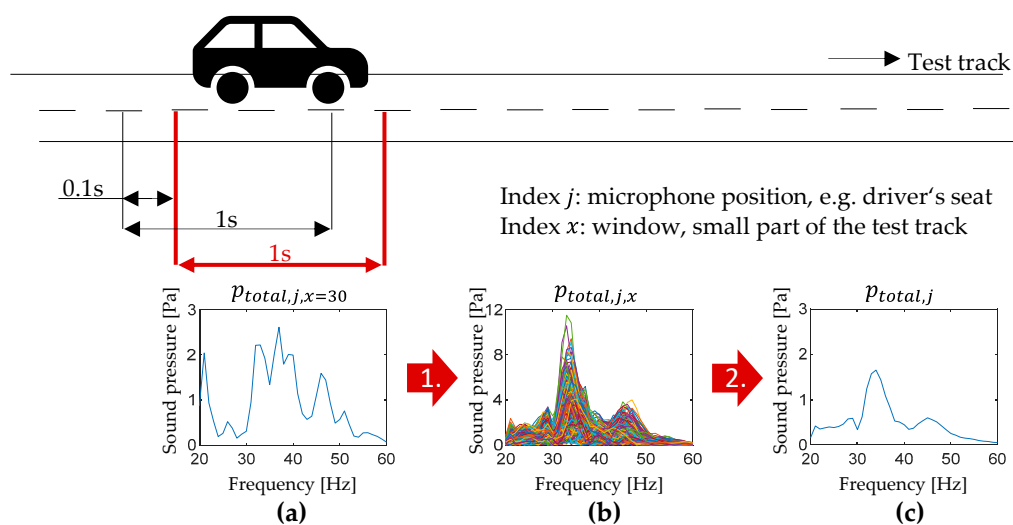


Figure 1. Method for calculating the sound pressure in the interior of a vehicle when driving over a test track, using a time segmentation of the excitation load approach: (a) Calculated sound pressure of one section; (b) Calculated sound pressure of all sections of the test track; (c) RMS average of all calculated sound pressures of all sections.

First, the track is divided into small windows, and then, each window is considered individually. Using one window as an example, the procedure for calculating the sound pressure is explained. Analogous to the previous method (see Section 2.3.1), the chassis internal forces are determined in the frequency domain. Multiplying the forces by the corresponding body transfer functions then yields a sound pressure for each transfer path. As a final step, the sound pressures are complexly summed in phase. The result is a total sound pressure $p_{total,j,x=30}$ that is obtained for the individual section of the track under consideration. The method is thus the same as the previous one (see Section 2.3.1), but it is done only for each window individually. The calculation of the total sound pressure

$p_{total, j, x}$ is then performed for each section of the track until the entire track has been calculated.

To be comparable with the results from the previous method (see Section 2.3.1), the same analysis parameters of the FFT used in the first approach must be chosen. Therefore, we split the track into windows with a length of one second and with an overlap of 90%.

As a last step, the total sound pressure of all windows is calculated using the following RMS averaging:

$$p_{total, j} = \sqrt{\frac{1}{x} \sum_{i=1}^x |p_{total, j, i}|^2} \quad (6)$$

The result is a total sound pressure $p_{total, j}$ resulting from the passage over the entire track. In contrast to the first method (see Section 2.3.1), in this approach the phase information about the vibrations of the rear axle is obtained for each section, since the calculation of the complex sound pressure is done for each window individually. With this approach, the averaging, and the resulting loss, of the phase information is only done at sound pressure level and not, already, at the internal chassis forces. This allows a much more precise description of the vibration behavior of the rear axle.

2.4. Simulation Models

This section presents the simulation models used to describe the transmission characteristics of the vehicle's body and the vibration behavior of the chassis. To use the elevation profile of the track (see Section 2.1) as an excitation in the time domain while keeping computation times low, we use a multibody simulation model for the chassis and powertrain model. For simulating the sound pressure level in the interior of a vehicle, an FE model of the body and air cavity is required and built. By combining the two simulation methods, we can calculate airborne sound with excitation in the time domain while keeping computation times low.

2.4.1. Vehicle's Body Simulation Model

The body simulation model consists of three sub-models for the vehicle structure, the trim, and the air cavities. Figure 2 shows the different sub-models.

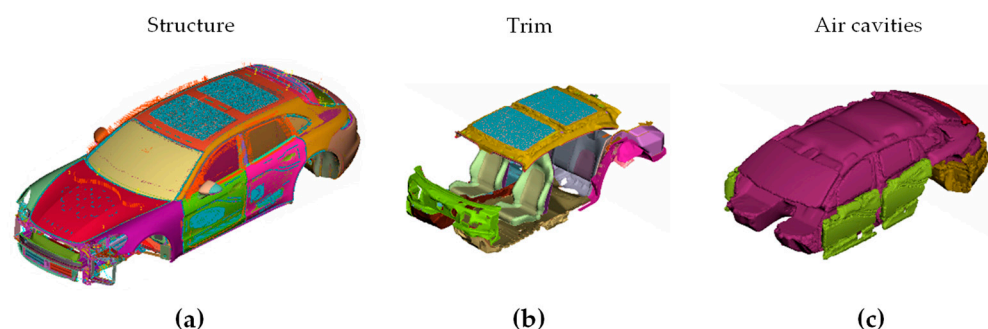


Figure 2. Trimmed body simulation model: (a) Structure model (FEM); (b) Trim (PEM); (c) Air cavities (FEM).

For the structural component of the trimmed body, we use a FE simulation model. All load-bearing structural components, as well as doors, hatches, and windows are included. The trim elements (seats, headliner, carpet, dash insulator, etc.) are modeled using PEM (poro-elastic finite elements method) and are integrated into the structural model. The air cavities, including the air inside the doors (light green), are part of the body model as well (tetrahedral elements TET10). The forced ventilation opening is connected to an air cavity in the rear of the vehicle between the trunk floor and the rear apron (dark green). More detailed information about state of the art simulation with PEM methods can be found in [17].

We export the modal parameters (invariant inertia matrix, mode shapes, and eigenfrequencies via Nastran v2017.2 SOL103 and the Craig-Bampton method [18]) of the FE structural model in a modal neutral file, which we then use for describing the coupling properties in a multibody simulation model.

2.4.2. Chassis and Powertrain Simulation Model

For the simulation of the complete vehicle, we build a multibody simulation model (MBS). It features the front axle, the rear axle, and the drivetrain. Figure 3 shows the model.

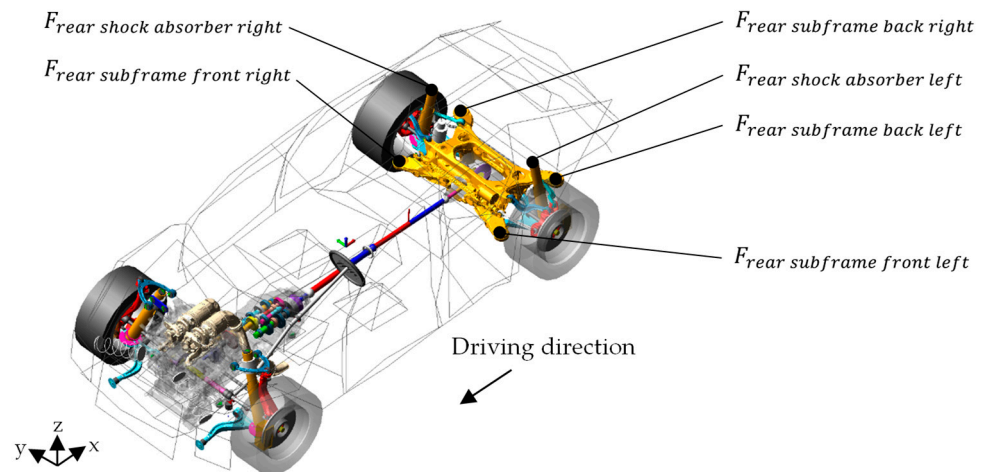


Figure 3. Chassis and powertrain simulation model (MBS).

The model is set up in MSC Adams/Car (version 2020.1) and uses a RMOD-K tire model [19]. The chassis and powertrain are coupled to a modal neutral file, which contains the structural elastic information of the finite element body model (see Section 2.4.1). The simulation model includes the entire powertrain, the chassis of the front and rear axles and the steering system, along with all chassis and powertrain bearings. The model is excited with the elevation profile of the test track and calculated in the time domain.

Since only the transfer paths of the rear axle (excluding the rear springs) are relevant for the description of road booming noise [8], only the six marked connection points of the chassis to the body are used. There are three directions per point, i.e., 18 internal forces.

3. Results

In this section, the results are presented. First, the two methods described (see Section 2.3), for combining internal chassis forces and body transfer functions, are compared based on measured data. Then, the best methodology is applied to simulation data.

3.1. Calculation of Road Booming Noise Based on Measured Data

As a first step, we compare the two approaches “averaging of the excitation spectrum” and “time segmentation of the excitation load” (see Section 2.3) for calculating the sound pressure level using chassis internal forces and body transfer functions. Figure 4 shows the results based on measured data.

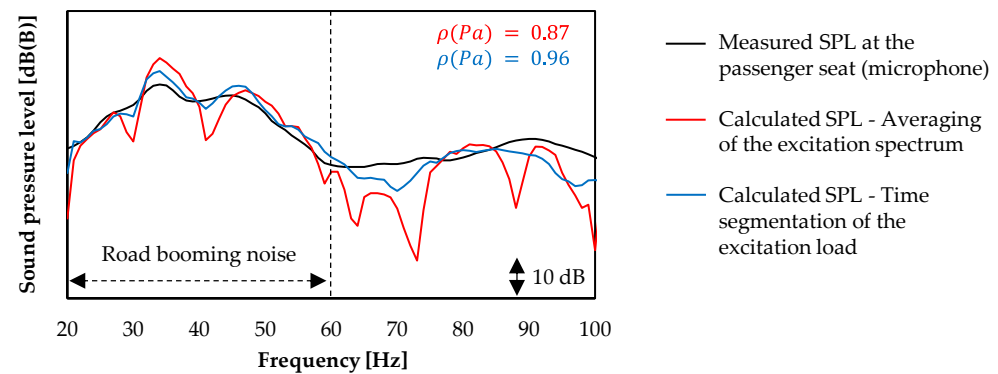


Figure 4. Comparison of the measured and calculated sound pressure level of a vehicle for driving on a rough road (test track, non-uniform road profile at 40 km/h).

The black curve represents the measured sound pressure level of a microphone at the head position on the front passenger seat. To account for low-frequency noise components, we use a B-weighting function. The calculated sound pressure level using the averaging of the excitation spectrum approach equals the red curve. Here, the chassis internal forces have been measured and determined simultaneously with the measurement of the sound pressure with the microphone. The blue curve corresponds to the time segmentation of the excitation load approach. The data used for the calculation of the sound pressure level for the two different approaches are the same.

In measured sound pressure levels, the wide maximum between 20 Hz and 60 Hz, consisting of two local maxima at 34 Hz and 45 Hz is clearly visible. The first approach (red) shows a similar curve to the measured sound pressure level, but has some sharp drops and is up to 7 dB(B) higher than the measurement at 34 Hz. The Pearson-correlation-coefficient, PCC, to the measured sound pressure based on the unit Pascal between 20 Hz and 100 Hz is 0.87. The mean absolute error, MAE, in the range of road booming noise between 20 Hz and 60 Hz is 0.15 Pa or 3.98 dB(B).

The result of the calculated sound pressure level for the second approach (blue) is much smoother and corresponds much better to the measured sound pressure than the first method. It can be clearly seen that especially the sharp drops are omitted. At the global maximum at 34 Hz, the calculated sound pressure is nevertheless up to 3 dB(B) higher than the measured one. The result of the calculation is improved by the second approach, compared to the first method, from 7 dB(B) to 3 dB(B) at the global maximum. The PCC based on the unit Pascal between 20 Hz and 100 Hz improves from 0.87 to 0.96. The MAE in the range of road booming noise between 20 Hz and 60 Hz is 0.07 Pa or 1.99 dB(B), which is 0.08 Pa and 1.99 dB(B) lower than with the “averaging of the excitation load spectrum” approach. There is no frequency deviation in the global maximum at 34 Hz for either method. In summary, the correlation of the calculated sound pressure level with the “time segmentation of the excitation load approach” is thus much higher than that of the “averaging of the excitation load spectrum approach” and can be rated as very high overall with a PCC of 0.96 and a MAE of 1.99 dB(B).

The clearly better result of the “time segmentation of the excitation load approach” is due to the fact that the phase correlations of the chassis forces are retained for each section of the track and the sound pressure is calculated in the correct phase for each section. In contrast to the “averaging of the excitation load approach”, this means that the data is only averaged at sound pressure level and not at force level. By averaging the phase relations on force level, a lot of information is lost, which leads to the lower result of the “averaging of the excitation load approach”. The mathematical difference of the two approaches is described in detail in Section 2.3.

With the “time segmentation of the excitation load approach”, we have now found a way to couple chassis forces with transfer functions of the vehicle’s body. This allows us to calculate the sound pressure when driving over a rough road with a very high correlation

to the measured sound pressure. For further investigations, we will now only pursue this approach and apply it to the simulation models.

3.2. Calculation of Road Booming Noise Using Simulation Data or a Hybrid Combination of Measurement and Simulation Data

In a first step, we will couple the sub-models for the chassis simulation and body simulation with measurement data from the respective other subsystem in order to evaluate the accuracy of the simulation models individually. Figure 5 shows the result.

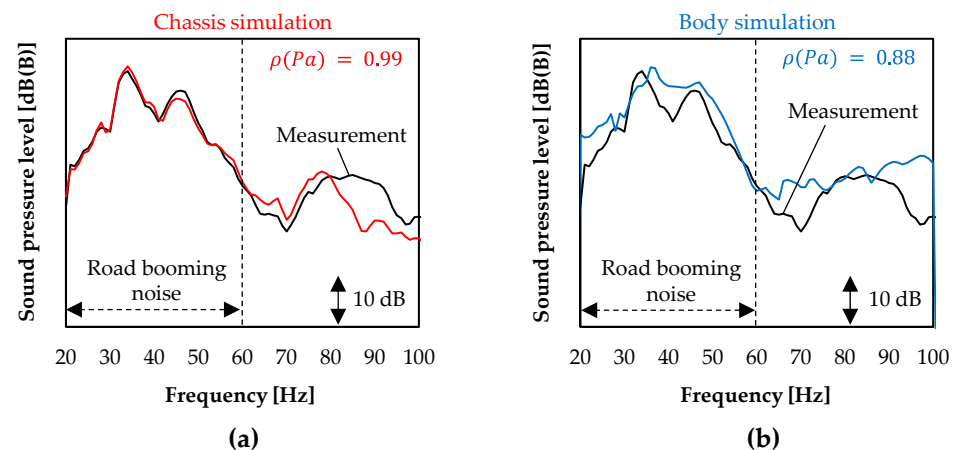


Figure 5. Calculated sound pressure level of a vehicle for driving on a rough road (test track, non-uniform road profile at 40 km/h): (a) Chassis simulation compared to the measurement; (b) Body simulation compared to the measurement.

The left diagram (a) shows in black the calculated sound pressure level based on test data. In comparison, the red curve shows the result of the chassis simulation model. For this purpose, the simulated internal forces from the MBS model (see Section 2.4.2) are coupled with measured transfer functions of the vehicle's body (see Section 2.2.1). The deviation is very low, especially in the area of road booming noise between 20 Hz and 60 Hz. At the global maximum, the difference is 0.9 dB(B). The PCC based on the unit Pa between 20 Hz and 100 Hz is 0.99. The MAE in the range of road booming noise between 20 Hz and 60 Hz is 0.06 Pa or 0.92 dB(B). Overall, the chassis simulation model shows very high correlation with the measured data, both qualitatively and quantitatively.

The right diagram (b) shows the result for the FE simulation of the vehicle's body (see Section 2.4.1). Again, the measurement is shown in black, and the calculated sound pressure level, which results from the combination of measured chassis internal forces (see Section 2.2.2) and simulated body transfer functions, is shown in blue. Since the entire body, including the trim elements and the air cavity, is more complex than the chassis model, the quality of the simulated sound pressure with the body simulation is slightly lower than with the chassis simulation model. The difference at the global maximum is 0.9 dB(B) and the PCC based on the unit Pa between 20 Hz and 100 Hz is 0.88. The MAE in the range of road booming noise between 20 Hz and 60 Hz is 0.29 Pa or 3.68 dB(B). Overall, the correlation of the body model is slightly lower than that of the chassis model, but still high.

In the next step, we combine the two simulation models for the chassis and the body. Figure 6 shows the calculated sound pressure level resulting from the coupling of both models, i.e., based purely on simulation data.

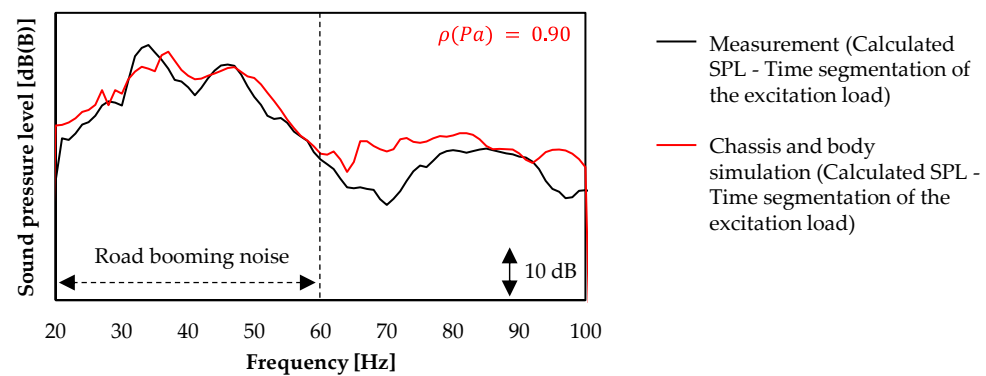


Figure 6. Comparison of the calculated sound pressure level of a vehicle for driving on a rough road (test track, non-uniform road profile at 40 km/h) based on measurements and based on a combination of a chassis and body simulation model (complete vehicle simulation model).

The black curve shows the calculated sound pressure based on measured data. The red curve displays the result of the complete vehicle simulation model, consisting of the chassis and body simulation model. The characteristic shape of the curves corresponds very well, especially in the low frequency range of road booming noise between 20 Hz and 60 Hz. The difference at the global maximum is 1.4 dB(B) and the PCC, based on the unit Pa between 20 Hz and 100 Hz, is 0.90. The MAE in the range of road booming noise between 20 Hz and 60 Hz is 0.19 Pa or 2.46 dB(B). Overall, the simulation model shows a very high correlation with the measured sound pressure from the test vehicle.

Based on the simulation models used and the “time segmentation of the excitation load” approach, we have succeeded in providing a simulated description of the booming noise behavior of a vehicle, which correlates very well with the measurement data gained on a test track with a test vehicle.

4. Conclusions

In this paper, we investigated different approaches for calculating sound pressures using chassis internal forces in combination with body transfer functions. We demonstrated that a time segmentation of the excitation load approach for the phenomenon road booming noise shows a very high correlation between the measured sound pressure of a microphone in the vehicle’s interior and the calculated sound pressure from the combination of individual transfer paths based on test data. At the same time, the results from Section 3.1 show that considering only the transfer paths of the rear axle (rear axle subframe and rear axle shock absorbers) is sufficient to describe road booming noise. These paths are crucial to calculate the sound pressure approximated to a microphone measurement. Using the time segmentation of the excitation load approach, we are now able to describe the booming behavior of a vehicle without an equivalent load case.

We then applied the methodology to our simulation models for the chassis and the vehicle’s body. In doing so, we can combine each of the individual models with measured data or combine the two simulation models for a complete vehicle simulation. Both the individual simulation models and the complete vehicle simulation show a very high correlation and low errors with the measured sound pressure level.

This paper thus demonstrates a method for using a combination of two simulations models and test data, either hybrid (combination simulation and measurement) or full digital (simulation models only), to compute and evaluate the booming behavior of a vehicle as it passes over a bad road.

Theoretically, a transfer of the methodology to other chassis-excited phenomena or even phenomena caused, e.g., via drive units, is conceivable and should be reviewed in the future. In addition, an extension of the frequency range is possible.

For further investigations, we will use the developed methodology and the simulation models to identify different influences on the booming behavior of a vehicle, based on parameter variations.

Author Contributions: Conceptualization, M.H., J.K. and W.S.; investigation, M.H., J.K. and W.S.; software, M.H.; writing—original draft preparation, M.H.; writing—review and editing, F.G.; visualization, M.H.; supervision, F.G. All authors have read and agreed to the published version of the manuscript.

Funding: This research was funded by Ing. h.c. F. Porsche AG within a cooperative project with Karlsruhe Institute of Technology (KIT), Institute of Vehicle System Technology.

Data Availability Statement: The data are not publicly available due to legal restrictions.

Acknowledgments: We acknowledge support by the KIT-Publication Fund of the Karlsruhe Institute of Technology. The authors are grateful for the NVH-Department of Ing. h.c. F. Porsche AG for supporting this work in collaboration with the Institute of Vehicle System Technology of the Karlsruhe Institute of Technology (KIT). Additionally, we thank A. Winandi from the Karlsruhe Institute of Technology for valuable input and support.

Conflicts of Interest: The authors declare no conflict of interest.

Abbreviations

The following abbreviations are used in the manuscript:

FEM	Finite Element Method
FFT	Fast Fourier Transformation
MAE	Mean Absolute Error
MBS	Multibody Simulation
NTF	Noise Transfer Function
NVH	Noise Vibration and Harshness
PCC	Pearson Correlation Coefficient
PEM	Poro-elastic Method
RMS	Root Mean Square
SPL	Sound Pressure Level

References

- Luegmair, M. *Simulation der Fahrzeugakustik in der Frühen Entwicklungsphase*; Springer: Aachen, Germany, 2016; p. 5.
- Mantovani, M. Rollgeräusche kann man nicht mit Emotionen verbinden. *Automob. Ztg.* **2018**, *120*, 18–21. [[CrossRef](#)]
- Rambacher, C.; Ehrh, T.; Sell, H. Schwingungsoptimierung ganzer Achsen. *Automob. Ztg.* **2017**, *119*, 54–59. [[CrossRef](#)]
- Ersoy, M.; Gies, S. *Fahrwerkhandbuch: Grundlagen Fahrdynamik Fahrverhalten Komponenten Elektronische Systeme Fahrerassistenz Autonomes Fahren Perspektiven*, 5th ed.; ATZ/MTZ-Fachbuch; Springer: Wiesbaden, Germany, 2017; ISBN 978-3-658-15467-7.
- Oh, S.-H.; Kim, H.; Park, Y. Active Control of Road Booming Noise in Automotive Interiors. *J. Acoust. Soc. Am.* **2002**, *111*, 180–188. [[CrossRef](#)] [[PubMed](#)]
- Kudritzki, D. Verfahren zur Analyse fahrwerkerregten Dröhnens im Pkw-Innenraum. In *Proceedings of the Tagung: Fahrzeuginnenraumakustik; Fahrzeuginnenraumakustik*: Essen, Germany, 1999.
- Brandstätter, M. Tieffrequente Geräusche in Einem Kraftfahrzeug bei Unebenheitsanregung. Ph.D. Thesis, Technische Universität Berlin, Berlin, Germany, 2013.
- Herrmann, M.; Jöst, R.; Kehl, F.; Özkan, A.; Pless, S.; Gauterin, F. Importance of Vehicle Body Elements and Rear Axle Elements for Describing Road Booming Noise. *Vehicles* **2020**, *2*, 589–603. [[CrossRef](#)]
- Genuit, K. *Sound-Engineering im Automobilbereich*; Springer: Berlin/Heidelberg, Germany, 2010; ISBN 978-3-642-01414-7.
- Uhlar, S. *Simulating and Optimizing the Dynamic Chassis Forces of the Audi E-Tron*; SAE Technical Paper 2020-01-1521; SAE: Warrendale, PA, USA, 2020. [[CrossRef](#)]
- Bijwe, V.; Raut, M.; Suryawanshi, S.; Naidu, S.; Titave, U.; Winney, G. *NVH Refinement of Passenger Vehicle for In-Cab Boom Noise Using Experimental Operational Deflection Shape and Full Vehicle Acoustic Sensitivity Simulations*; SAE: Warrendale, PA, USA, 2011.
- Sung, S.; Chao, S.; Lingala, H.; Mundy, L. *Structural-Acoustic Analysis of Vehicle Body Panel Participation to Interior Acoustic Boom Noise*; SAE: Warrendale, PA, USA, 2011.
- Zeller, P. *Handbuch Fahrzeugakustik: Grundlagen, Auslegung, Berechnung, Versuch*, 3rd ed.; ATZ/MTZ-Fachbuch; Springer: Wiesbaden, Germany, 2018; ISBN 978-3-658-18519-0.
- Mitschke, M.; Wallentowitz, H. *Dynamik der Kraftfahrzeuge*; Springer: Wiesbaden, Germany, 2014; ISBN 978-3-658-05067-2.

15. Kemna, J. Analyseverfahren auf Bauteil-und Systemebene zur Bewertung von Gummi-Metall-Lagern in Bezug auf Fahrkomfort und Fahrdynamik. Ph.D. Thesis, Institut für Mechanik und Mechatronik, Wien, Austria, 2018. [[CrossRef](#)]
16. Hallez, R.; Vansant, K. A Case Study for Predicting Wind Noise inside a Car Compartment Using a Multi-Disciplinary CFD and Acoustic Approach. In Proceedings of the ISMA 2014 including USD 2014, KU Leuven, Dep. Werktuigkunde, Leuven, Belgium, 17 September 2014; pp. 301–316.
17. Caillet, A.; Blanchet, D. Status on State of the Art in PEM Simulation in the Automotive Industry. In Proceedings of the 41st Deutsche Jahrestagung für Akustik (DAGA), Nürnberg, Germany, 16–19 March 2015.
18. Craig, R.R.; Bampton, M.C.C. Coupling of Substructures for Dynamic Analyses. *AIAA J.* **1968**, *6*, 1313–1319. [[CrossRef](#)]
19. Oertel, C.; Fandre, A. Das Reifenmodellsystem RMOD-K. *ATZ* **2001**, *103*, 1074–1079. [[CrossRef](#)]